European Journal of
Mineralogy
Open Access

# Tancaite-(Ce), ideally FeCe(MoO$_4$)$_3$ · 3H$_2$O: description and average crystal structure

**Elena Bonaccorsi**[1,2] **and Paolo Orlandi**[1]

[1]Earth Science Department, University of Pisa, Pisa, 56126, Italy
[2]CISUP, Centro per l'Integrazione della Strumentazione dell'Università di Pisa, Pisa, 56126, Italy

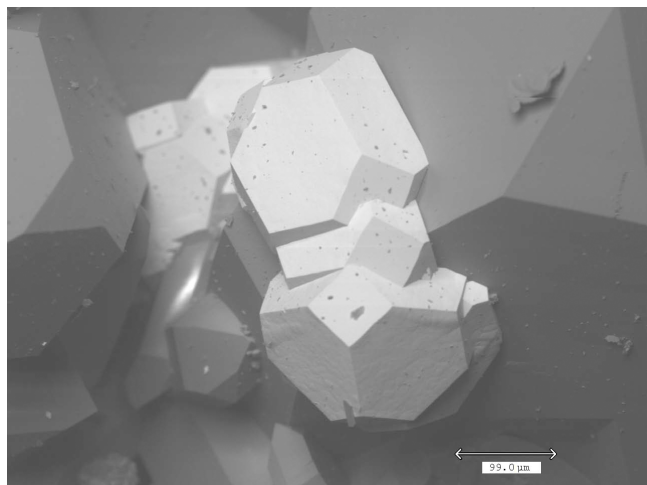**Correspondence:** Elena Bonaccorsi (elena.bonaccorsi@unipi.it)

**Abstract.** Tancaite-(Ce), ideally FeCe(MoO$_4$)$_3$·3H$_2$O, is a new mineral occurring within cavities in the quartz veins which cut the granite at Su Seinargiu, Sarroch (CA), Sardinia, Italy. It is a secondary mineral formed in the oxidation zone of a sulfide ore vein. Associated minerals are quartz, muscovite, molybdenite, pyrite, and a mendozavilite-like phase. Tancaite-(Ce) is red or pale brown in colour, with a vitreous to adamantine lustre. Electron microprobe analyses give (wt %) SiO$_2$ 0.34, CaO 0.09, Fe$_2$O$_3$ 11.29, SrO 0.02, La$_2$O$_3$ 5.04, Ce$_2$O$_3$ 10.35, Pr$_2$O$_3$ 1.07, Nd$_2$O$_3$ 3.66, Sm$_2$O$_3$ 0.19, ThO$_2$ 2.58, UO$_2$ 0.17, MoO$_3$ 58.62, and H$_2$O (calculated) 7.43, with a sum of 100.85, from which the empirical formula is calculated. The empirical formula Fe$^{3+}_{1.03}$(Ce$_{0.46}$La$_{0.23}$Nd$_{0.16}$Pr$_{0.05}$Sm$_{0.01}$U$_{0.01}$Th$_{0.07}$)$_{\Sigma=0.99}$(Mo$_{2.96}$Si$_{0.04}$)$_{\Sigma=3.00}$O$_{12}$·3H$_2$O can be simplified as Fe$^{3+}$(REE)(MoO$_4$)$_3$·3H$_2$O and idealized as FeCe(MoO$_4$)$_3$·3H$_2$O. The presence of H$_2$O was confirmed by micro-Raman spectrometry (stretching and bending vibrations of O–H). The calculated density is 3.834 g cm$^{-3}$. The X-ray diffraction pattern of tancaite-(Ce) is characterized by a set of strong reflections, which point to a cubic subcell with $a = 6.870(1)$ Å and space group $Pm\bar{3}m$, plus a set of superstructure reflections. Tancaite-(Ce) displays a new structure type not previously reported in natural and synthetic molybdates. By considering only the strong reflections, it was possible to solve and refine its average structure ($R1 = 0.038$ for 192 unique reflections with $I > 2\sigma(I)$). The crystal structure consists of FeO$_6$ octahedra centred at the origin of the cubic subcell and linked together through MoO$_4$ tetrahedra by corner sharing. The Mo-centred tetrahedra are statistically distributed in four symmetry-related positions, with one-fourth occupancy. In the centre of the cubic unit cell the REE cations exhibit a $6 + 3$ coordination, bonding six oxygen atoms and three H$_2$O molecules, each of them being disorderly distributed in four symmetry-related positions. One of the possible supercells, with a 48-fold volume with respect to the primitive cubic small subcell, corresponded to a rhombohedral lattice, with $a \approx 19.43$ and $c \approx 47.60$ Å in the hexagonal setting. Several unsuccessful trials were performed to solve the real crystal structure of tancaite, by indexing the additional superstructure reflections and using their intensities to refine an ordered structural model. The new mineral has been approved by the IMA CNMNC (no. 2009-097). The name comes from Giuseppe Tanca, an Italian amateur mineralogist, who discovered the mineral and gave it to us for studying.

## 1 Introduction

Tancaite-(Ce) occurs in cavities in quartz veins within granite at Su Seinargiu, Sarroch (CA), Sardinia, Italy. It is a secondary mineral formed in the oxidation zone of a sulfide ore vein. Associated minerals are quartz, muscovite, molybdenite, pyrite, and a mendozavilite-like mineral (Orlandi et al.,

2013). More than 60 different mineral species have been described from this locality (Orlandi et al., 2015d); among them and in addition to tancaite-(Ce), another seven minerals have Su Seinargiu as the type locality: sardignaite (Orlandi et al., 2010), gelosaite (Orlandi et al., 2011), mambertiite (Orlandi et al., 2015c), susenargiuite (Orlandi et al., 2015b), ichnu-

**Figure 1.** SEM photograph showing truncated octahedra of tancaite-(Ce).

**Table 1.** Chemical data for tancaite-(Ce).

| Constituent | wt % | Range | Elements | a.p.f.u.[a] |
|---|---|---|---|---|
| $SiO_2$ | 0.34 | 0.02–1.56 | Si | 0.04 |
| CaO | 0.09 | 0.03–0.14 | Ca | 0.00 |
| $Fe_2O_3$ | 11.29 | 11.04–11.71 | $Fe^{3+}$ | 1.03 |
| SrO | 0.02 | 0.00–0.07 | Sr | 0.00 |
| $La_2O_3$ | 5.04 | 4.66–5.53 | La | 0.23 |
| $Ce_2O_3$ | 10.35 | 9.47–11.15 | Ce | 0.46 |
| $Pr_2O_3$ | 1.07 | 0.88–1.35 | Pr | 0.05 |
| $Nd_2O_3$ | 3.66 | 2.50–4.19 | Nd | 0.16 |
| $Sm_2O_3$ | 0.19 | 0.08–0.34 | Sm | 0.01 |
| $ThO_2$ | 2.58 | 1.97 3.44 | Th | 0.07 |
| $UO_2$ | 0.17 | 0.00–0.29 | U | 0.01 |
| $MoO_3$ | 58.62 | 57.50–59.59 | Mo | 2.96 |
| $H_2O$[b] | 7.43 | | H | 6.00 |
| Total | 100.85 | | | |

[a] Number of atoms per formula unit, based on 15 O. [b] $H_2O$ was calculated on the basis of the structural data, which point to three $H_2O$ molecules per formula unit.

saite (Orlandi et al., 2014), nuragheite (Orlandi et al., 2015a), and cabvinite (Orlandi et al., 2017).

The new mineral has been approved by the IMA Commission on New Minerals, Nomenclature and Classification (no. 2009-097). The name honours Giuseppe Tanca (b. 1943), an amateur mineralogist with invaluable experience in the mineralogy of Sardinia who first found tancaite-(Ce). The Levinson modifier is in line with the dominance of $Ce^{3+}$ among the REEs. The holotype of tancaite-(Ce) has been deposited in the collections of the Natural History Museum, University of Pisa, catalogue no. 18911.

## 2　Appearance and physical properties

The mineral generally occurs as small truncated octahedra (Fig. 1), up to 0.2 mm in size, red or pale brown in colour, transparent, with vitreous to adamantine lustre. It displays a yellow streak and is not fluorescent. Its Mohs hardness is 4 to 4.5; it is brittle and shows conchoidal fracture. Cleavage and parting are not observed.

The calculated density is $3.834\,\mathrm{g\,cm^{-3}}$, based on the empirical formula. Such a high value prevented us from measuring density by means of tungsten-based heavy liquids. Weak birefringence was observed, but the high indices of refraction, with average $n_{calc} = 1.90$ (Mandarino, 1981), and the scarcity of material did not allow for a complete optical characterization. Twinning at a small scale is probable (see the structural description), but it is not observed macroscopically.
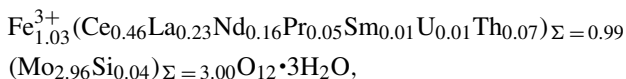
## 3　Chemical data

Chemical analyses (10) were carried out by using an ARL-SEMQ electron microprobe (wavelength-dispersive-

spectroscopy electron probe microanalyser, WDS-EPMA) at the University of Modena and Reggio Emilia (Italy). Operating conditions were as follows: voltage of 15 kV, beam current of 20 nA, and beam diameter of 20 μm. We used the following as standards: synthetic Sr-anorthite (Sr), cerussite (Pb), synthetic phosphates for the rare earths (La, Ce, Pr, Nd, Sm), $ThO_2$ (Th), UCoSi (U), ilmenite (Fe), glass (Si, Ca), and $CaMoO_4$ (Mo). Lead was sought but not detected. $H_2O$ was calculated by stoichiometry from the results of the crystal-structure analysis. Analytical data are given in Table 1. The empirical formula (based on 15 O atoms) is

$$Fe^{3+}_{1.03}(Ce_{0.46}La_{0.23}Nd_{0.16}Pr_{0.05}Sm_{0.01}U_{0.01}Th_{0.07})_{\Sigma=0.99}$$
$$(Mo_{2.96}Si_{0.04})_{\Sigma=3.00}O_{12}\cdot 3H_2O,$$

which may be simplified as $Fe^{3+}(REE)(MoO_4)_3 \cdot 3H_2O$. Because of the predominant Ce among the REE cations, the end-member formula is $FeCe(MoO_4)_3 \cdot 3H_2O$, which requires $Fe_2O_3$ 10.94, $Ce_2O_3$ 22.49, $MoO_3$ 59.16, $H_2O$ 7.41, and total 100.00 wt %.

To confirm the presence of $H_2O$ molecules, non-polarized micro-Raman spectra were collected at the Department of Physics and Earth Sciences of the University of Parma, Italy. They were obtained in near-backscattered geometry with a Jobin Yvon Horiba LabRAM apparatus, equipped with a motorized $x-y$ stage and an Olympus microscope with a ×50 objective. Three different regions of the micro-Raman spectrum are shown in Fig. 2. The Raman peaks of the low-wavenumber region (Fig. 2a) can be related to stretching and bending modes of the $MO_4$ groups (Frost et al., 2007). The band around $1620\,\mathrm{cm^{-1}}$ (Fig. 2b) corresponds to the O–H bending mode, whereas the band at $3430\,\mathrm{cm^{-1}}$ (Fig. 2c) corresponds to the O–H stretching mode.
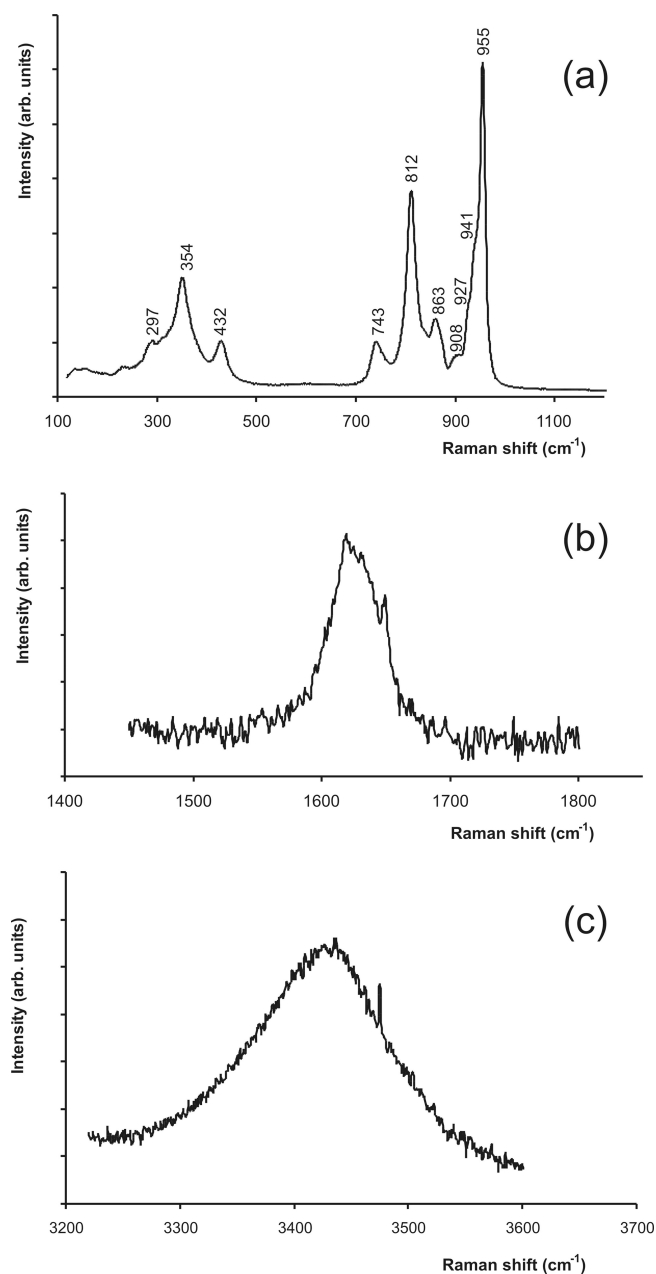
**Figure 2.** Micro-Raman spectra of tancaite-(Ce). The band around 1620 cm$^{-1}$ (**b**) corresponds to the O–H bending mode, whereas the band at 3430 cm$^{-1}$ (**c**) corresponds to the O–H stretching mode.

## 4  X-ray diffraction studies

A very preliminary X-ray investigation of tancaite-(Ce) using oscillating-crystal, Weissenberg, and Gandolfi techniques indicated that the reflections could be indexed based on a small cubic unit cell with $\approx 6.87$ Å. However, long exposed photographs and successive data collections revealed several weaker reflections, suggesting that a larger unit cell was needed to correctly index them.

By measuring only the first set of reflections with a P4 Siemens four-circle diffractometer, and graphite-monochromatized Mo$K\alpha$ radiation, it was possible to solve and refine the "average structure" of tancaite in space group $Pm\bar{3}m$ up to a reliability index $R = 0.062$ for 149 unique reflections. The structural model was successively improved through high-resolution intensity data collection and anisotropic refinement. The description of this average structure is reported in the next section.

In order to obtain the real unit cell and symmetry of tancaite-(Ce), several intensity data collections were performed for three different crystals, selected from the same hand specimen, in different experimental settings and by using both conventional X-ray sources and synchrotron radiation. Two data collections were performed on the same crystal used to solve the average structure. The former was performed at the synchrotron facility Elettra, at the XRD1 beamline; the latter was carried out by means of an Oxford diffractometer equipped with a charge-coupled device (CCD), operating with Mo$K\alpha$ radiation (CRIST Laboratory, University of Florence, Italy). One of the possible supercells showed trigonal symmetry, with $R$-centred lattice, $a \approx 19.4$, and $c \approx 47.6$ Å in the hexagonal setting. Two other unit cells were equally possible, the former corresponding to an $F$-centred cubic cell with $a \approx 27.5$ Å, and the latter corresponding to an $I$-centred tetragonal cell with $a \approx 19.4$ Å and $c \approx 27.5$ Å. The low intensity of the measured additional reflections did not allow for a clear symmetry attribution based on the $R_{int}$ indices, which were very similar for cubic (0.099), trigonal (0.098), and tetragonal (0.098) systems.

Another data collection was carried out for another crystal of tancaite-(Ce) with a CCD-equipped Oxford diffractometer, operating with Mo$K\alpha$ radiation (CIADS Laboratory, University of Sienna, Italy). In this case, the superstructure reflections indicated a smaller unit cell, orthorhombic $C$-centred with $a = 19.286(1)$, $b = 27.246(1)$, $c = 9.6331(5)$. Finally, a new data collection was performed on a third crystal of tancaite-(Ce). The data were collected in our laboratory, with a Bruker SMART BREEZE diffractometer equipped with an air-cooled CCD detector using graphite-monochromatized Mo$K\alpha$ radiation. Three datasets of 963 frames were collected in 0.5° slices with an exposure time of 45 s. The detector-to-crystal working distance was set to 50 mm. Data were integrated and corrected for Lorentz and polarization, background effects, and absorption using Apex 2 (Bruker AXS Inc., 2016), resulting in 10 314 unique reflections in space group $R\bar{3}$ with $a = 19.2901(3)$, $c = 47.2510(5)$. Other possible supercells were detected, as in the preceding trials. A possible symmetry of the ordered phase will be discussed in the next section, whereas a list of the possible supercells and the matrices to obtain them from the small cubic cell with $a = 6.87$ Å are reported in Table 2.

X-ray powder-diffraction data were obtained using a 114.6 mm diameter Gandolfi camera and Cu$K\alpha$ radiation. The pattern was initially indexed on the basis of the cu-

**Table 2.** Different possible unit cells, as derived from the X-ray diffraction patterns of tancaite-(Ce). In the first row, the subcell common to all the patterns is reported; in the last column the transformation matrices, which related the different unit cells to the common subcell, are listed. For the possible real symmetry of tancaite-(Ce), see the text.

| $a$ (Å) | $b$ (Å) | $c$ (Å) | $\alpha$ (°) | $\beta$ (°) | $\gamma$ (°) | Lattice | Matrix |
|---|---|---|---|---|---|---|---|
| 6.87 | 6.87 | 6.87 | 90 | 90 | 90 | $P$ | 100/010/001 |
| 19.43 | 19.43 | 47.60 | 90 | 90 | 120 | $R$ | 2-20/02-2/444 |
| 27.48 | 27.48 | 27.48 | 90 | 90 | 90 | $F$ | 400/040/004 |
| 19.43 | 19.43 | 27.48 | 90 | 90 | 90 | $I$ | 2-20/220/004 |
| 19.43 | 27.48 | 9.72 | 90 | 90 | 90 | $C$ | 2-20/004/110 |

**Table 3.** Powder X-ray data for of tancaite-(Ce). The refined unit cell is $a = 19.305(1)$, $c = 47.438(5)$, and space group $R\bar{3}$. The eight strongest reflections are reported in bold.

| $h$ | $k$ | $l$ | $d_{calc}$ | $d_{obs}$ | $I_{rel}$ |
|---|---|---|---|---|---|
| **2** | **2** | **0** | **4.83** | **4.84** | **45** |
| **0** | **4** | **2** | **4.12** | **4.12** | **8** |
| **4** | **0** | **4** | **3.94** | **3.93** | **75** |
| 4 | 1 | 3 | 3.55 | 3.56 | 5 |
| **0** | **4** | **8** | **3.42** | **3.42** | **100** |
| 0 | 1 | 14 | 3.32 | 3.33 | 2 |
| 4 | 2 | 2 | 3.13 | 3.14 | 6 |
| 2 | 4 | 4 | 3.05 | 3.04 | 6 |
| 1 | 5 | 5 | 2.863 | 2.849 | 3 |
| **0** | **6** | **0** | **2.786** | **2.785** | **10** |
| 4 | 4 | 0 | 2.413 | 2.410 | 5 |
| 2 | 6 | 2 | 2.307 | 2.305 | 3 |
| 6 | 2 | 4 | 2.275 | 2.275 | 3 |
| 2 | 6 | 8 | 2.159 | 2.159 | 6 |
| 8 | 0 | 2 | 2.082 | 2.085 | 4 |
| 0 | 8 | 4 | 2.058 | 2.059 | 3 |
| 8 | 0 | 8 | 1.971 | 1.967 | 3 |
| 4 | 2 | 20 | 1.897 | 1.899 | 5 |
| **2** | **8** | **0** | **1.824** | **1.825** | **15** |
| 4 | 4 | 18 | 1.780 | 1.782 | 1 |
| 5 | 6 | 2 | 1.748 | 1.745 | < 1 |
| 7 | 4 | 0 | 1.734 | 1.733 | < 1 |
| 0 | 8 | 16 | 1.708 | 1.708 | 7 |
| 10 | 0 | 4 | 1.655 | 1.655 | 5 |
| **6** | **6** | **0** | **1.609** | **1.610** | **10** |
| 6 | 2 | 22 | 1.579 | 1.579 | 1 |
| 9 | 3 | 0 | 1.546 | 1.546 | < 1 |
| 4 | 8 | 8 | 1.527 | 1.528 | 2 |
| 10 | 2 | 8 | 1.455 | 1.456 | 1 |
| 2 | 10 | 10 | 1.431 | 1.432 | 1 |
| **2** | **10** | **16** | **1.339** | **1.340** | **12** |
| 4 | 8 | 20 | 1.315 | 1.315 | 3 |
| 2 | 2 | 36 | 1.271 | 1.270 | 3 |
| 2 | 12 | 8 | 1.246 | 1.247 | 3 |

bic subcell. However, even in the powder diffraction pattern some weak reflections were not indexed on the basis of this unit cell. The large trigonal $R$-centred unit cell was used to completely index it (Table 3), using the method of

Holland and Redfern (1997) on the basis of eight unequivocally indexed reflections, and the refined cell parameters were $a = 19.305(1)$, $c = 47.438(5)$, and $V = 15\,311(3)$ Å$^3$ assuming the space group $R\bar{3}$.

## 5   Solution and refinement of the average structure

The substructure of tancaite-(Ce) was solved by direct methods with SHELXS-97 (Sheldrick, 2008) by using the strong reflections indexed on the basis of the small cubic cell with $a = 6.870(1)$ and $V = 324.2(1)$ Å$^3$. The space group is $Pm\bar{3}m$ and the structure was refined up to $R1 = 0.038$ for 200 unique reflections with the SHELX programme (Sheldrick, 2015). Scattering curves for neutral atoms were taken from the International Tables for X-ray Crystallography (Wilson, 1992).

The crystal structure consists of FeO$_6$ octahedra (dark grey, Fig. 3) centred at the origin of the cubic cell and linked together through MoO$_4$ tetrahedra by corner sharing (Fig. 3a). The molybdate tetrahedra are statistically distributed in four symmetry-related positions, with one-fourth occupancy (Fig. 3b). The $Ce$ site is in the centre of the unit cell, and it is actually occupied by REEs; however, the scattering factor of Ce was used during all the structural refinement steps. The oxygen atoms (black spheres in Fig. 3a) coordinated by the Ce cation are 24 in number. However, the one-fourth occupancy of the oxygen sites, related to the occupancy of the Mo cations, points to an average of six O atoms coordinated by each Ce atom. In addition to those, H$_2$O molecules are located within the cavity, in a general position with multiplicity 24, at a distance of 2.54 Å from the Ce cation. The occupancy of H$_2$O sites was allowed to vary in the early refinement cycles, obtaining a site occupancy factor very close to one-eighth. Based on the H$_2$O site scattering power, and in agreement with the low sum of analysed constituents in microprobe data (Table 1), we conclude that three H$_2$O molecules statistically occur within the cavity. Therefore, the Ce cations exhibit 6 + 3 coordination, with six oxygen atoms and three H$_2$O molecules.
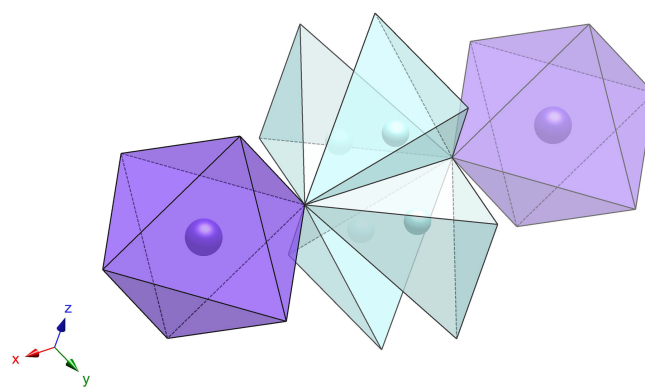
The four possible positions for the MoO$_4^{2-}$ groups are shown in Fig. 4, having O2–O2 as the common edge. Crystal data and structure refinement parameters are listed in Table 4.
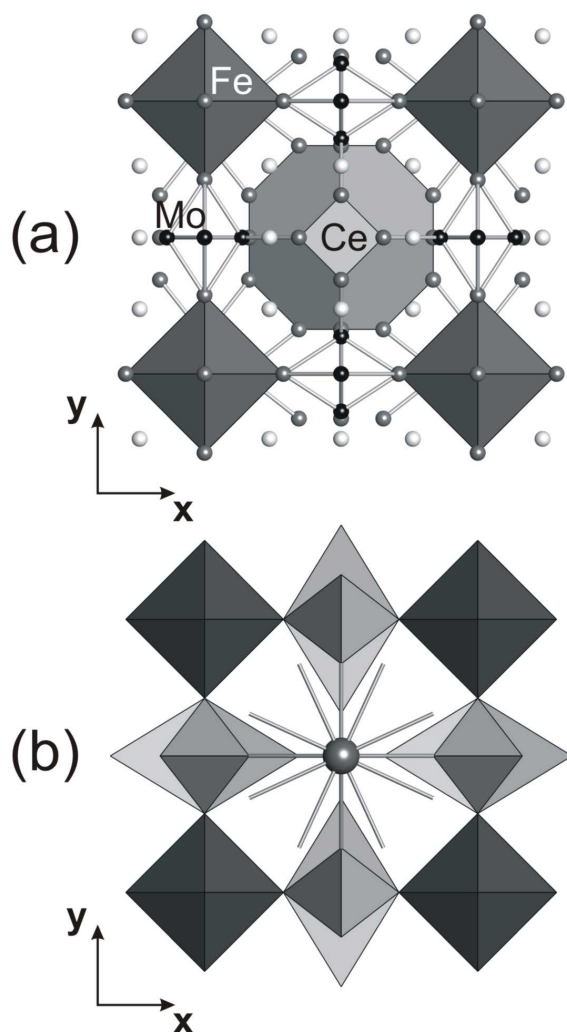
**Figure 3.** Crystal structure of tancaite-(Ce) in space group $Pm\bar{3}m$; **(a)** the Ce cation lies within the light grey polyhedron; $Fe^{3+}$-centred octahedra are indicated in dark grey; partially occupied Mo, O, and $H_2O$ sites are indicated, respectively, by black, grey, and white spheres; **(b)** the molybdate groups are statistically distributed over four possible and mutually exclusive positions, related by the fourfold axis (light grey tetrahedra); the ligands of the Ce cation are shown.



**Figure 4.** Connection of two Fe-centred octahedra by means of a molybdate group, which may statistically occur in four possible orientations.
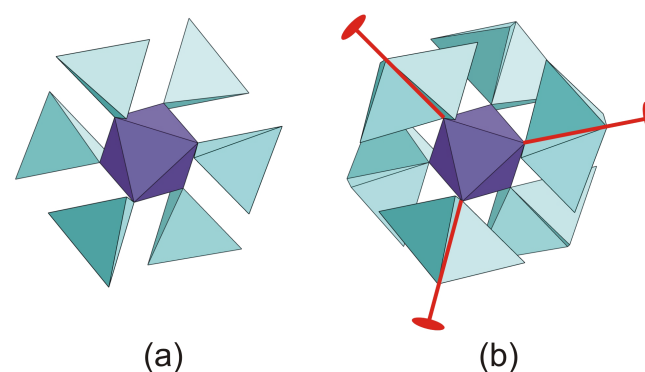


**Figure 5.** In **(a)** a possible ordering scheme is sketched for the orientations of the $MoO_4$ tetrahedra around to a $FeO_6$ octahedron, which is compatible with a threefold axis. Such ordering cannot occur in the cubic, tetragonal, or orthorhombic unit cells which index the superstructure reflections, as reported in Table 2. The effect of twofold axes is shown in **(b)**.

Atom positions and bond distances are given in Tables 5 and 6, respectively.

The refined structure is clearly an average structure, characterized by statistical positional disorder which involves both the Mo cations and the ligands of the Ce cations at the centre of the unit cell. Several attempts to refine this average structure in lower symmetry space groups, by partial ordering of the $MoO_4$ groups, did not result in significant improvement of the reliability index. Moreover, additional electron density maxima always occurred approximately in the same positions of the high-symmetry model.

On the basis of the structural data, we hypothesize that the real structure of tancaite-(Ce) displays an ordered arrangement of $MoO_4$ orientations, with a consequent ordering of the Ce ligands inside the cubic cage. Such ordering schemes result in the occurrence of superstructure reflections which correspond to one or more multiple cells with respect to the cubic disordered one. We can confidently exclude that a completely ordered structure may be realized in cubic, tetragonal, and orthorhombic systems. In particular, the occurrence of fourfold as well as twofold axes implies a disordered distribution of the orientations of the $MoO_4$ tetrahedra connecting the $FeO_6$ octahedra. The effect of twofold axes may be appreciated in Fig. 5. Additionally, the cubic symmetry is not in agreement with the birefringence observed in the study of the optical properties.

Among the possible supercells which were sought in order to index the weak superstructure reflections, we therefore suggest the trigonal one with a rhombohedral lattice as the

**Table 4.** Crystal data and structure refinement parameters for tancaite-(Ce). In the second column the available data are reported for the average structure of tancaite-(Ce), whereas in the third column the unit cell and symmetry for the real structure of tancaite-(Ce) are indicated, as refined on the basis of X-ray powder diffraction data.

| | | |
|---|---|---|
| Empirical formula | CeFe(MoO$_4$)$_3$ 3H$_2$O | |
| Formula weight | 729.84 | |
| Wavelength | 0.71073 Å | |
| Crystal system | Cubic | Trigonal |
| Space group | $Pm\bar{3}m$ | $R\bar{3}$ |
| Unit cell dimensions | $a = 6.870(1)$ Å | $a = 19.2901(3)$, $c = 47.2510(5)$ |
| Volume | 324.2(1) Å$^3$ | 15226.9(7) Å$^3$ |
| $Z$ | 1 | 48 |
| Density (calculated) | 3.738 Mg m$^{-3}$ | |
| Absorption coefficient | 7.427 mm$^{-1}$ | |
| $F(000)$ | 336 | |
| Crystal size | $0.1 \times 0.08 \times 0.08$ mm$^3$ | |
| Theta range for data collection | 2.97 to 36.14° | |
| Index ranges | $-11 \leq h \leq 11$ | |
| | $-11 \leq k \leq 11$ | |
| | $-11 \leq l \leq 8$ | |
| Reflections collected | 3757 | |
| Independent reflections | 200 [$R_{\text{int}} = 0.0719$] | |
| Completeness to theta $= 36.14°$ | 100.0 % | |
| Absorption correction | Semi-empirical from equivalents | |
| Max. and min. transmission | 0.552 and 0.495 | |
| Refinement method | Full-matrix least squares on $F^2$ | |
| Data/restraints/parameters | 200/0/20 | |
| Goodness of fit on $F^2$ | 1.261 | |
| Final $R$ indices [$I > 2\sigma(I)$] | $R1 = 0.0387$, $wR2 = 0.0792$ | |
| $R$ indices (all data) | $R1 = 0.0424$, $wR2 = 0.0815$ | |
| Largest diff. peak and hole | 0.714 and $-0.832e\cdot$Å$^{-3}$ | |

**Table 5.** Site occupancies, atom coordinates, and equivalent displacement parameters in the average cubic structure of tancaite-(Ce).

| | Site multiplicity | Occupancy | $x/a$ | $y/b$ | $z/c$ | $U_{\text{eq}}$ |
|---|---|---|---|---|---|---|
| Ce | 1 | 1 | 0.5 | 0.5 | 0.5 | 0.022(1) |
| Fe | 1 | 1 | 0.0 | 0.0 | 0.0 | 0.013(1) |
| Mo | 12 | 1/4 | −0.1377(2) | 0.5 | 0.0 | 0.016(1) |
| O1 | 24 | 1/4 | −0.342(3) | 0.5 | 0.836(2) | 0.072(6) |
| O2 | 6 | 1 | 0.0 | 0.1290(1) | 0.0 | 0.046(2) |
| H$_2$O | 24 | 1/8 | −0.236(2) | 0.5 | 0.764(2) | 0.034(4) |

most likely because it allows us to build a completely ordered structural model. Anyway, any trial to refine it against measured diffraction intensities failed because of strong pseudo-symmetry problems. All the examined crystals are probably twinned, simulating a pseudo-cubic symmetry. It is also possible that domains with partially disordered structures may occur in the same crystal, at a very fine scale. A transmission electron microscopy study could possibly confirm this hypothesis.

## 6 Relation to other species

Tancaite-(Ce) belongs to class 49 in the Dana classification (basic and hydrated molybdates and tungstates hydrated), whereas in the Nickel and Strunz classification it belongs to 7.GB (molybdates with additional anions and/or H$_2$O).

Whereas a great number of synthetic molybdate compounds are known, there are relatively few molybdate minerals and none of the natural molybdates have close structural relationships with tancaite-(Ce). On the contrary, tancaite-(Ce) is related to the crystal structure of Fe$_2$(MoO$_4$)$_3$, a synthetic compound which displays interesting magnetic and thermal properties, including negative thermal expan-

**Table 6.** Selected bond distances in the average cubic structure of tancaite-(Ce).

| Ce-O1 | 2.553(17) × 6 | Fe-O2 | 1.993(7) × 6 | Mo-O1 | 1.799(17) × 2 |
|---|---|---|---|---|---|
| Ce-H$_2$O | 2.561(17) × 3 | | | Mo-O2 | 1.724(6) × 2 |
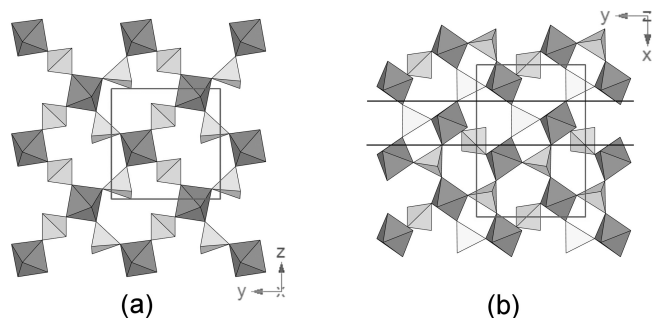


**Figure 6. (a)** Structural layer in Fe$_2$(MoO$_4$)$_3$, as seen down [100]; **(b)** connection of layers as in **(a)**, as seen down [001].

sion (Harrison, 1995). The orthorhombic crystal structure of Fe$_2$(MoO$_4$)$_3$ can be described as being formed by (100) layers as depicted in Fig. 6a, which may be obtained from those described in the average structure of tancaite-(Ce) (see Fig. 3b) through a positional ordering of the molybdate groups and some distortions. In the synthetic Fe$_2$(MoO$_4$)$_3$ these layers are linked together along [100] by sharing the apical oxygen atoms of the Fe-centred octahedra of one layer with an oxygen atom of the (MoO$_4$) tetrahedra of an adjacent layer (Fig. 6b). In contrast, the topologically similar layers of tancaite-(Ce) are connected through the insertion of additional MoO$_4$ tetrahedra, giving rise to wider cavities which can host the REE cations and the H$_2$O molecules.

From another point of view, the crystal structure of tancaite-(Ce) could be described as a derivative of the perovskite structure. Analogous to the description of the crystal structure of several high-temperature superconductors, in which "perovskite-like layers" are separated by layers with different geometries and compositions, here we have "interlayer" (MoO$_4$) groups, which separate the perovskite-like units (namely the octahedra) in all the three directions $x$, $y$, and $z$. The result appears as an "expanded" perovskite structure, similar to some hybrid perovskites intercalated with organic molecules (Li et al., 2017).

## 7   Conclusions

The new mineral tancaite-(Ce) displays a new structure type not previously reported in natural and synthetic molybdates. Its average structure is cubic and corresponds to an expanded perovskite structure in which Fe-centred octahedra are connected to each other through MoO$_4$ tetrahedra showing orientational disorder. By assuming a completely ordered structure, it is possible to build a structural model in one of the

observed supercells, with trigonal symmetry and $R$-centred lattice. However, it was not possible to refine it using the weak intensities of the superstructure reflections, probably because domains with different degrees of order may occur in the same crystal, possibly in a twinning relationship.

Natural and synthetic molybdates are of a great practical interest due to their thermal properties, as several of them show interesting negative thermal expansion. Moreover, they are also investigated for their ionic conductivity and possible usefulness for immobilization of radionuclides. Additional studies are therefore needed to investigate the behaviour of tancaite-(Ce) upon changing temperature and chemical environment.

## References

Bonaccorsi, E. and Orlandi, P.: Tancaite-(Ce) data set, CIF and FCF files, figshare, https://doi.org/10.6084/m9.figshare.12319214, 2020.

Bruker AXS Inc.: APEX 3. Bruker Advanced X-ray Solutions, Madison, WI, USA, 2016.

Frost, R. L., Bouzaid, J., and Butler, I. S.: Raman spectroscopic study of the molybdate mineral szenicsite and compared with other paragenetically related molybdate minerals, Spectrosc. Lett., 40, 603–614, https://doi.org/10.1080/00387010701301220, 2007.

Harrison, W. T. A.: Crystal structure of paraelastic aluminum molybdate and ferric molybdate, $\beta-Al_2(MoO_4)_3$ and $\beta-Fe_2(MoO_4)_3$, Mat. Res. Bull., 30, 1325–1331, https://doi.org/10.1016/0025-5408(95)00157-3, 1995.

Holland, T. J. B. and Redfern, S. A. T.: Unit cell refinement from powder diffraction data: the use of regression diagnostics, Mineral. Mag., 61, 65–77, https://doi.org/10.1180/minmag.1997.061.404.07, 1997.

Li, W., Wang, Z., Deschler, F., Gao, S., Friend, R. H., and Cheetham, A. K.: Chemically diverse and multifunctional hybrid organic–inorganic perovskites, Nature Rev. Mat., 2, 16099, https://doi.org/10.1038/natrevmats.2016.99, 2017.

Mandarino, J. A.: The Gladstone-Dale relationship; Part IV, The compatibility concept and its application, Can. Mineral., 19, 441–450, 1981.

Orlandi, P., Pasero, M., and Bigi, S.: Sardignaite, a new mineral, the second known bismuth molybdate: description and crystal structure, Mineral. Petrol., 100, 17–22, https://doi.org/10.1007/s00710-010-0111-0, 2010.

Orlandi, P., Demartin, F., Pasero, M., Leverett, P. Williams, P. A., and Hibbs, D. E.: Gelosaite, $BiMo^{6+}_{(2-5x)}Mo^{5+}_{6x}O_7(OH)\cdot H_2O$ $(0 \leq x \leq 0.4)$, a new mineral from Su Senargiu (CA), Sardinia, Italy, and a second occurrence from Kingsgate, New England, Australia, Am. Mineral., 96, 268–273, https://doi.org/10.2138/am.2011.3597, 2011.

Orlandi, P., Gelosa, M., Bonacina, E., Caboni, F., Mamberti, M., Tanca, G. A., and Vinci, A.: Sardignaite, gelosaite et tancaite-(Ce): trois nouveaux mineraux de Su Seinargiu, Sarroch, Sardigne, Italie, Une minéralisation à molibdéne avec bismuth et terres rares, Le Regne Mineral, 112, 39–52, 2013.

Orlandi, P., Biagioni, C., Bindi, L., and Nestola, F.: Ichnusaite, $Th(MoO_4)_2\cdot 3H_2O$, the first natural thorium molybdate: occurrence, description, and crystal structure, Am. Mineral., 99, 2089–2094, https://doi.org/10.2138/am-2014-4844, 2014.

Orlandi, P., Biagioni, C., Bindi, L., and Merlino, S.: Nuragheite, $Th(MoO_4)_2\cdot H_2O$, the second natural thorium molybdate and its relationships to ichnusaite and synthetic $Th(MoO_4)_2$, Am. Mineral., 100, 267–273, https://doi.org/10.2138/am-2015-5024, 2015a.

Orlandi, P., Biagioni, C., Moëlo, Y., Langlade, J., and Faulques, E.: Suseinargiuite, $(Na_{0.5}Bi_{0.5})MoO_4$, the Na-Bi analogue of wulfenite, from Su Seinargiu, Sardinia, Italy, Eur. J. Mineral., 27, 695–699, https://doi.org/10.1127/ejm/2015/0027-2463, 2015b.

Orlandi, P., Biagioni, C., Pasero, M., Demartin, F., Campostrini, I., and Merlino, S.: Mambertiite, $BiMo^{5+}_{2.80}O_8(OH)$, a new mineral from Su Seinargiu, Sardinia, Italy: occurrence, crystal structure, and relationships with gelosaite, Eur. J. Mineral., 27, 405–415, https://doi.org/10.1127/ejm/2015/0027-2434, 2015c.

Orlandi, P., Gelosa, M., Bonacina, E., Caboni, F., Mamberti, M., Tanca, G. A., and Vinci, A.: Sette nuove specie mineralogiche dalla Sardegna, I minerali della mineralizzazione a molibdeno e bismuto di Su Seinargiu (CA), Rivista Mineralogica Italiana, 39, 84–115, 2015d.

Orlandi, P., Biagioni, C., and Zaccarini, F.: Cabvinite, $Th_2F_7(OH)\cdot 3H_2O$, the first natural actinide halide, Am. Mineral., 102, 1384–1389, https://doi.org/10.2138/am-2017-6013, 2017.

Sheldrick, G. M.: A short history of SHELX, Acta Crystallogr., A64, 112–122, https://doi.org/10.1107/S0108767307043930, 2008.

Sheldrick, G. M.: Crystal structure refinement with SHELXL, Acta Crystallogr., C71, 3–8, https://doi.org/10.1107/S2053229614024218, 2015.

Wilson, A. J. C. (Ed.): International Tables for Crystallography, Volume C: Mathematical, physical and chemical tables, Kluwer Academic, Dordrecht, NL, 1992.